

We are IntechOpen, the world's leading publisher of Open Access books Built by scientists, for scientists

6,900

Open access books available

186,000

International authors and editors

200M

Downloads

Our authors are among the

154

Countries delivered to

TOP 1%

most cited scientists

12.2%

Contributors from top 500 universities



WEB OF SCIENCE™

Selection of our books indexed in the Book Citation Index
in Web of Science™ Core Collection (BKCI)

Interested in publishing with us?
Contact book.department@intechopen.com

Numbers displayed above are based on latest data collected.
For more information visit www.intechopen.com



Fiber Laser for Phase-Sensitive Optical Time-Domain Reflectometry

Vasily V. Spirin, Cesar A. López-Mercado,
Patrice Mégret and Andrei A. Fotiadi

Additional information is available at the end of the chapter

<http://dx.doi.org/10.5772/intechopen.72553>

Abstract

We have designed a new fiber laser configuration with an injection-locked DFB laser applicable for phase-sensitive optical time-domain reflectometry. A low-loss fiber optical ring resonator (FORR) is used as a high finesse filter for the self-injection locking of the DFB (IL-DFB) laser. By varying the FORR fidelity, we have compared the DFB laser locking with FORR operating in the under-coupled, critically coupled, and over-coupled regimes. The critical coupling provides better frequency locking and superior narrowing of the laser linewidth. We have demonstrated that the locked DFB laser generates a single-frequency radiation with a linewidth less than 2.5 kHz if the FORR operates in the critically coupled regime. We have employed new IL-DFB laser configuration operating in the critical coupling regime for detection and localization of the perturbations in phase-sensitive OTDR system. The locked DFB laser with a narrow linewidth provides reliable long-distance monitoring of the perturbations measured through the moving differential processing algorithm. The IL-DFB laser delivers accurate localization of the vibrations with a frequency as low as ~50 Hz at a distance of 9270 m providing the same signal-to-noise ratio that is achievable with an expensive ultra-narrow linewidth OEwaves laser (OE4020-155000-PA-00).

Keywords: fiber laser, self-injection locking, phase-sensitive OTDR

1. Introduction

Distributed fiber optic sensors are widely used for variety of applications such as structural health monitoring, perimeter and pipeline security, temperature, pressure, strain, and vibration measurements due to its lightweight, ease of installation, and immunity to electromagnetic fields [1–18]. One of the modern forward-looking fiber optic techniques, the so-called phase-sensitive

optical time-domain reflectometry (φ -OTDR), enables detection of acoustical perturbations along sensing optical fibers of several kilometers length [19–22].

Such optical sensor analyzer operates as a conventional OTDR, where a light pulse is injected into the optical fiber and Rayleigh backscattering radiation originating from the natural refractive index inhomogeneities frozen in the fiber core is recorded as time-dependent traces. However, in contrast to the conventional OTDR utilizing low coherence laser sources and hence based on recording of Rayleigh backscattering intensity, the φ -OTDR systems require highly coherent lasers with a coherence length exceeding the pulse duration and employ a difference between consequent time-dependent traces as a readout signal. For proper operation of φ -OTDR systems, the allowed optical frequency shift between two neighboring pulses should be low enough to keep Rayleigh backscattering interference pattern recorded as a result of pulse reflections from multiple scattering fiber centers unchangeable. Under these conditions, two consecutive traces recorded in an undisturbed fiber are identical. Meanwhile, any change in geometry of the frozen distribution of the refractive index in the fiber core caused by stress, strain, or temperature variations applied to some fiber points affects the difference between successive traces and, therefore, can be detected and localized with φ -OTDR systems [19–22]. Typically for long-distance measurements, a coherent laser source with a few kHz linewidth and frequency drift less than 1 MHz/min is required [2].

It is well known that self-injection locking of conventional telecom DFB lasers could significantly improve their spectral performance [23–34]. In our previous works, we have demonstrated substantial narrowing of the laser linewidth due to a spectrally selective feedback realized with FORR built from low-cost standard fiber telecom components [35–37]. To provide the DFB laser locking, a part of the optical radiation emitted by the DFB laser is passed through the filtering in a fiber ring resonator and returned into the laser cavity. This low-cost all-fiber solution allows achieving the laser linewidth as narrow as 500 Hz [36].

In this chapter, we demonstrate application of the DFB laser locked through a fiber ring cavity for φ -OTDR systems. In particular, we show that the proposed laser solution in combination with the moving differential processing algorithm enables accurate detection and localization of vibrations applied to the sensing fiber at a distance up to 10 km.

2. Experimental results and discussion

Figure 1 shows the experimental configuration of the DFB laser locked through a fiber optic ring resonator (FORR). The MITSUBISHI FU-68PDF-V520M27B DFB laser with a built-in optical isolator operates a linewidth of ~ 2 MHz at the wavelength of ~ 1534.85 nm. The output DFB laser radiation is passed through an optical circulator (OC), optical coupler (C1), and polarization controller (PC1) and then introduced into a fiber optic ring resonator. The FORR consists of a variable ratio coupler VRC, 95/5 coupler C2 and comprises ~ 4 m length of a standard SMF-28 fiber. The operation of FORR is similar to the Fabry-Perot interferometer

with the reflected power detected in port B and transmitted power directed to the coupler C3 [20]. The radiation at the port A is used as an output of the injection-locked DFB (IL-DFB) laser, while port B and C are connected to detectors for the monitoring of the reflected and transmitted powers, respectively. Optical isolators prevent reflections from the fiber ends that potentially could affect the DFB laser behavior. The polarization controller (PC2) and the optical switcher (OS) are used to adjust the feedback strength and activate or deactivate the optical feedback loop that returns transmitted through the FORR power back into the DFB laser cavity.

Once the DFB laser frequency gets a resonance with the FORR, the DFB laser is locked in frequency to one of the FORR frequency modes. This effect could be observed as a suppression of the temporal power fluctuations recorded at ports C and B. **Figure 2** shows typical oscilloscope traces of transmitted and reflected powers recorded at ports C and B, respectively. Single

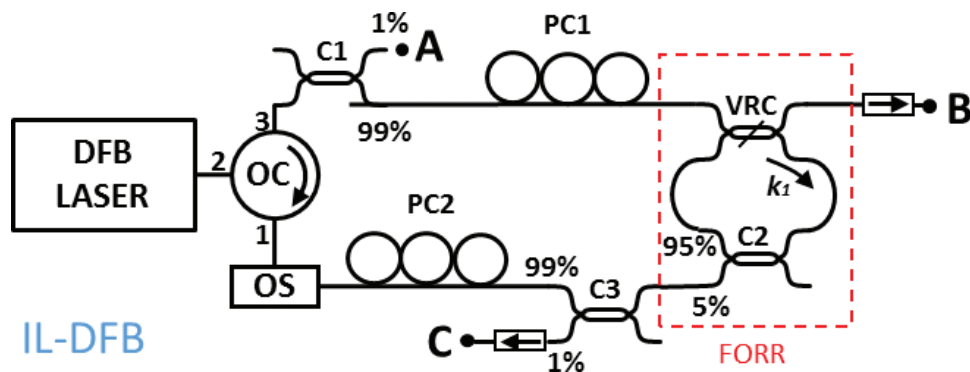


Figure 1. The experimental configuration of the DFB laser locked through FORR. OC—Optical circulator, VRC—Variable ratio coupler, C—Optical coupler, PC—Polarization controller, OS—Optical switcher.

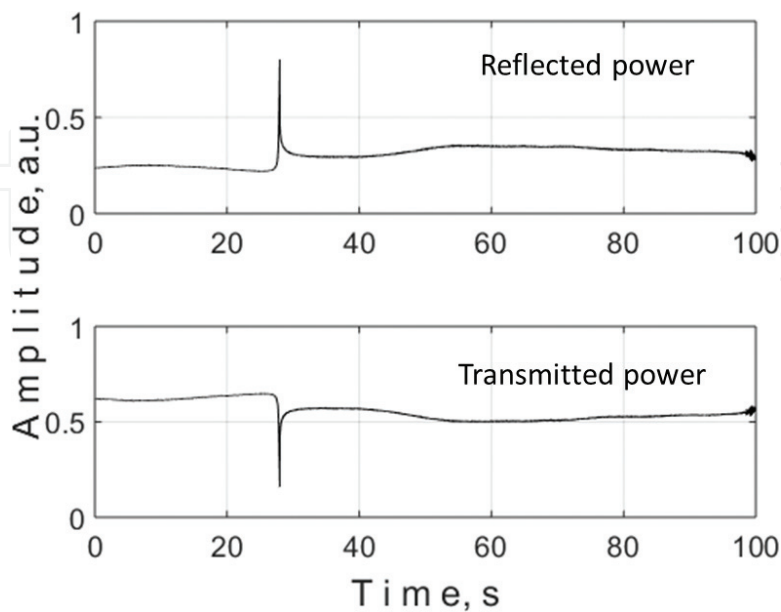


Figure 2. Typical oscilloscope traces for transmitted and reflected powers.

frequency regime is observed during some time intervals that are interrupted by short-time mode hopping events. The frequency drift during the stable time interval strongly depends on environmental conditions and can be less than 1–2 MHz/min, if the FORR is placed in an isolation box used for environmental protection.

Stabilization of the laser operation is accompanied by stabilization of the polarization state of the locked DFB laser radiation recorded at the port A and the transmitted power recorded at the port C (see **Figure 3**). However, during the mode hopping, the polarization state can be changed. In our previous work, we have reported two possible regimes of mode hopping [35]. The first regime, we have attributed to the hopping between FORR modes of nearest orders, but of the same polarization state, and the second one to the hopping between orthogonal polarizations modes of the same order. These two regimes have significantly different time which the system takes to recover steady-state operation after the mode hopping event. In the first most common regime, the recovery time is typically ~ 5 ms, but in the second regime, the typical recovery time is significantly less and equal to ~ 100 μ s [35].

The locking performance strongly depends on the parameters of the VRC coupler used in the FORR. The coupling regime is defined by a relation between the VRC coupling coefficient k_1 and the total losses inside the cavity α [38]:

$$\begin{aligned} k_1 < 1 - \alpha(1 - \gamma_1) & \text{ under-coupling regime,} \\ k_1 = 1 - \alpha(1 - \gamma_1) & \text{ critical-coupling regime,} \\ k_1 > 1 - \alpha(1 - \gamma_1) & \text{ over-coupling regime,} \end{aligned} \quad (1)$$

where the power transmission coefficient α includes all losses inside the fiber loop and γ_1 is the intensity loss in the variable ratio coupler.

Figure 4 shows the normalized reflected power versus the coupling coefficient k_1 at port B. In the critical coupling regime, the reflected power reaches the minimum, and therefore, all nearby input power are transmitted through the FORR (see **Figure 5**). For that reason, the critical coupling provides higher feedback strength leading to better locking.

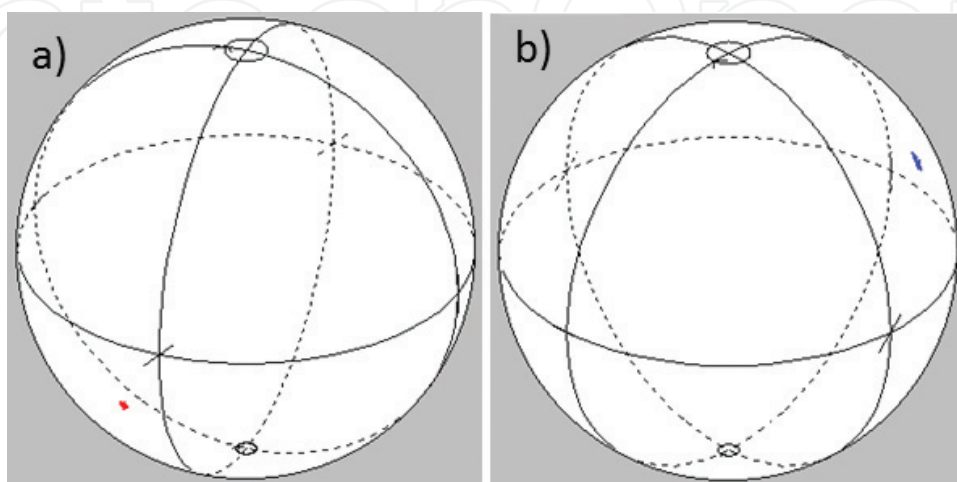


Figure 3. Polarization behavior during the stable interval: a) at port a and b) at port C.

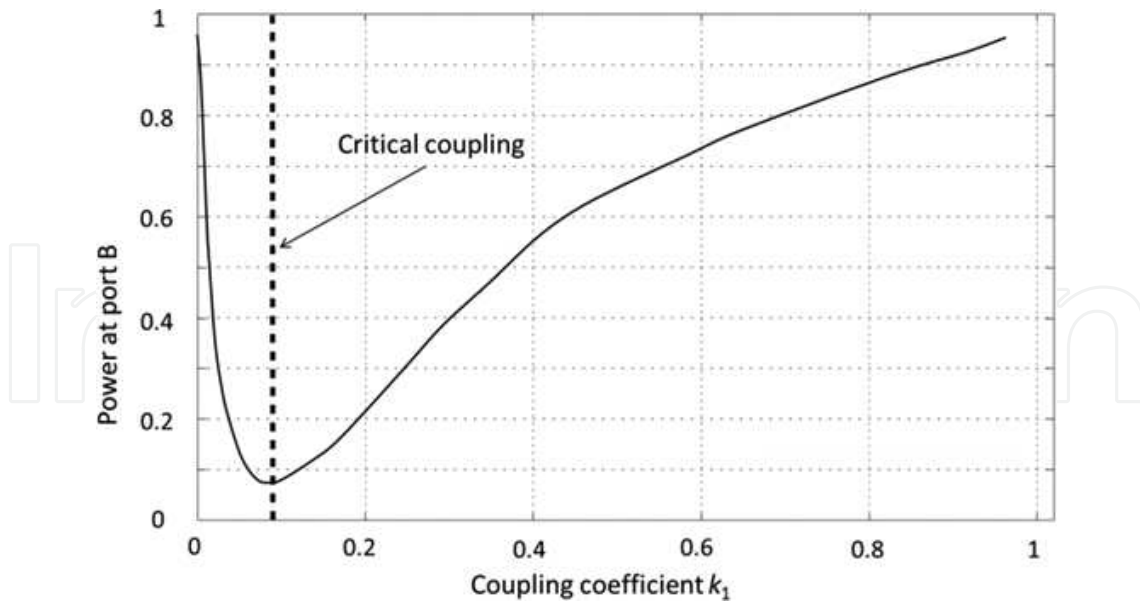


Figure 4. Normalized reflected power versus coupling coefficient k_1 at port B.

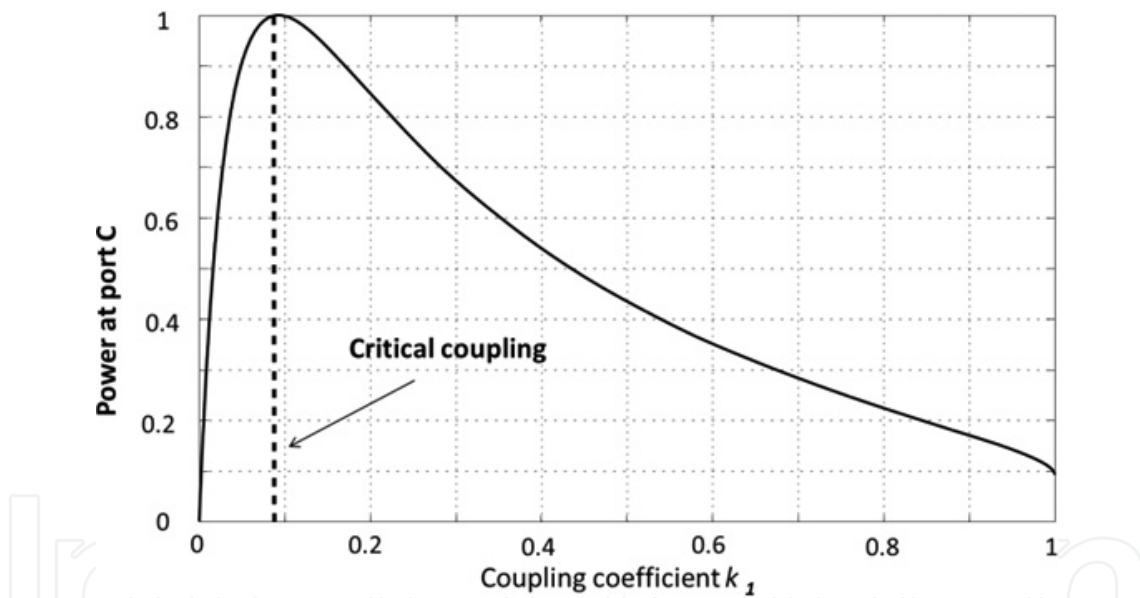


Figure 5. Normalized transmitted power versus coupling coefficient k_1 at port C.

Let us stress out that for the DFB laser locked at the resonance frequency of the FORR, the transmitted and reflected powers from FORR are in good agreement with the theoretical estimations.

The finesse of the resonance peak of the FORR is defined as a ratio of the FORR intermode interval to the spectral peak width:

$$\mathcal{F} = FSR/\Delta f \quad (2)$$

where $FSR = c/nL \approx 50$ MHz is the free spectral range of the FORR and Δf is the full-width at half-maximum (FWHM) of the feedback loop transmission peak.

For the FORR configuration with an additional coupler C2, Δf could be found following the same procedure as it is described in Ref. 26 for a simple optical ring resonator. For our resonator, the FWHM of the cavity mode can be estimated as [37]:

$$\Delta f = \frac{1}{2\pi\tau} \cos^{-1} \left(2 - \frac{1 + \alpha(1 - \gamma_1)(1 - k_1)}{2\sqrt{\alpha(1 - \gamma_1)(1 - k_1)}} \right) \quad (3)$$

In the critical coupling regime at $k_1 = 0.08$, Eq. (3) gives $\Delta f = 0.77$ MHz and the finesse $\mathcal{F} = 65.8$.

The finesse of the resonator strongly depends on the total cavity losses and the coupling coefficient. The finesse is higher for smaller losses and lower coupling coefficients (see **Figure 6**).

The delayed self-heterodyne spectra of the IL-DFB laser measured with unbalanced Mach-Zehnder interferometer [39] during the time intervals of stable laser operation at the critical coupling regime are shown in **Figure 7**. The Mach-Zehnder interferometer comprises 35 km of the delay fiber line in one arm and 20 MHz phase modulator in the other. The beat signal of two interferometer arms is detected by 125 MHz photodiode and RF spectrum analyzer. One can see that the DFB laser linewidth $\Delta\nu$ decreases from approximately 2 MHz for a free running laser to 2.4 kHz for the IL-DFB laser operating in critical coupling regime.

Assuming the Lorentzian shape of the laser line, the laser coherence length L_c [40] is described as:

$$L_c = \frac{c}{\pi N_{eff} \Delta\nu} \quad (4)$$

where c is the speed of the light in vacuum, N_{eff} is the effective group refraction index in the sensing fiber equal to 1.468 [41], and $\Delta\nu$ is the laser linewidth.

Therefore, the coherence length is increased from approximately 26 m for a free running DFB laser up to 27.2 km for the IL-DFB laser operating in the critical coupling regime.

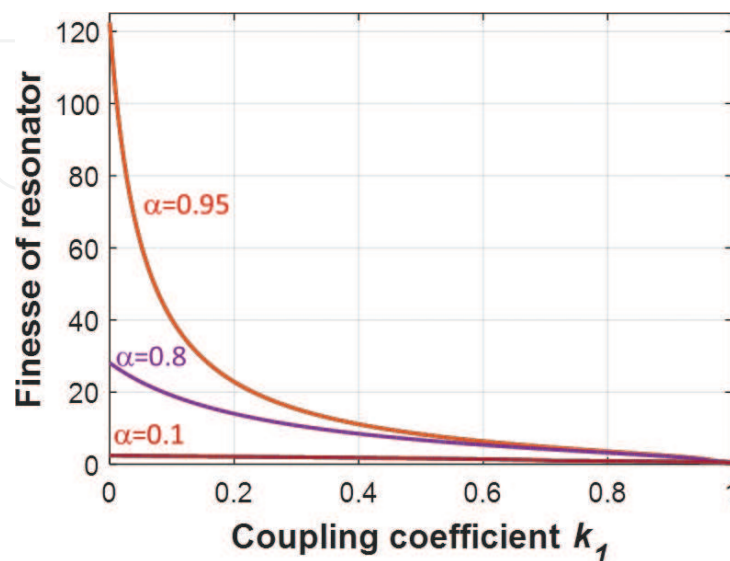


Figure 6. The finesse of resonator versus coupling factor k_1 .

Figure 8 shows the experimentally measured linewidth of the locked DFB laser versus the coupling coefficient k_1 . The minimal linewidth of about 2.5 kHz is achieved for the laser operating in the under-coupling and critical coupling regimes. In the over-coupling regime, the laser linewidth significantly increases.

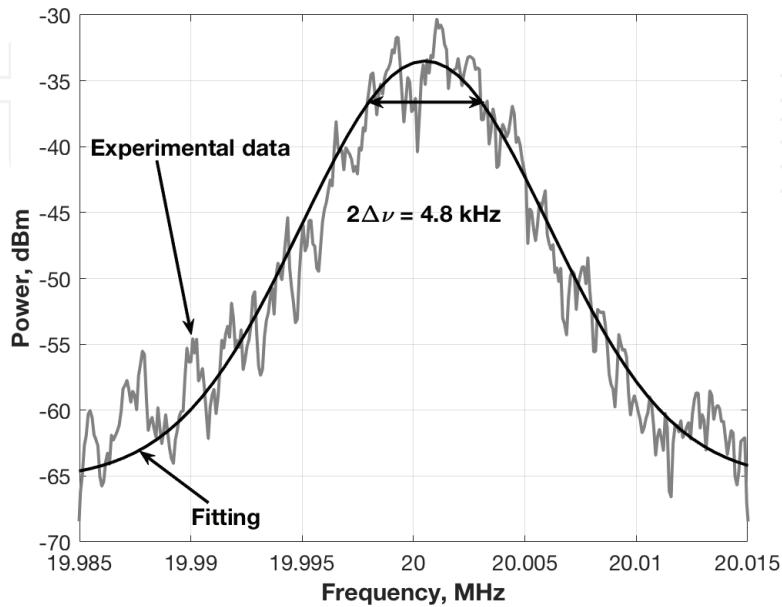


Figure 7. Delayed self-heterodyne spectra of the IL-DFB laser recorded with the laser stabilized for operation in the critical coupling regime.

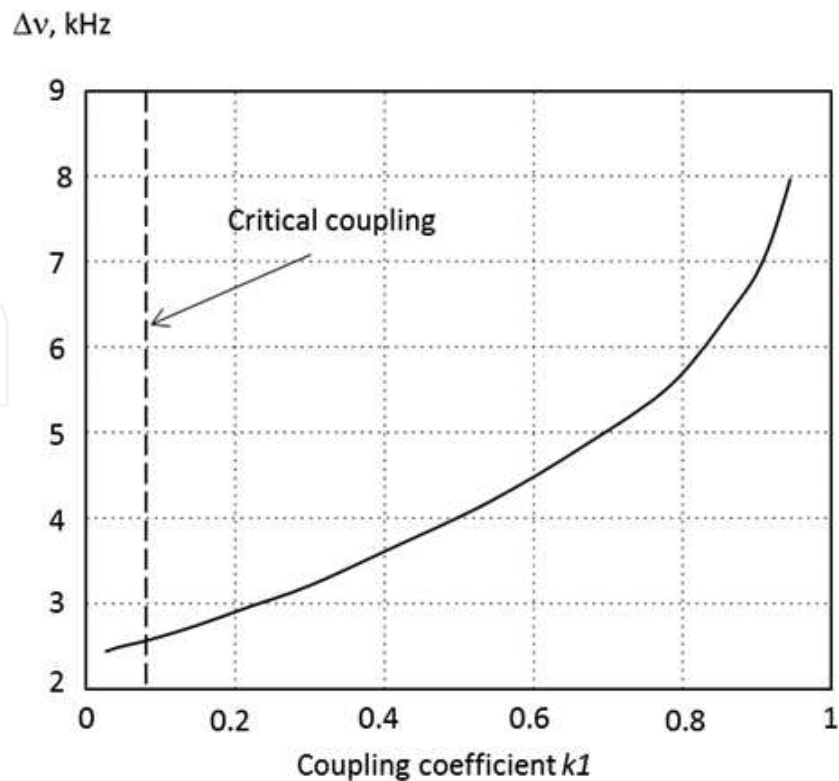


Figure 8. Experimental linewidth of the locked DFB laser versus the coupling coefficient k_1 .

Thus, the critical coupling provides the best IL-DFB laser stability and narrowest linewidth making the laser applicable in φ -OTDR systems.

The configuration of the φ -OTDR system with IL-DFB laser operating in the critical coupling regime is shown in **Figure 9**. The output radiation of the IL-DFB laser is amplified by an EDFA up to 23 mW and passes through a bandpass filter (BPF) to filter out spontaneous emission noise.

An optical intensity modulator (OIM) provides generation of optical pulses with the width of 350 ns and repetition rate of 10 kHz introduced into the sensing fiber through 1/99 coupler and an optical circulator. The sensing fiber comprises 8400 m of standard SMF-28e and 950 m of Raman Optical Fiber (OFS) with the loss coefficient of about 0.33 dB/km. Acoustic perturbations at the frequency of 50 Hz are generated at the sensing fiber distance of 9270 m by a loudspeaker.

The Rayleigh backscattered signal traces have been detected at the port E by 125 MHz photodetector and recorded by an oscilloscope. Each from about 1024 similar traces of 100 ms length has been digitized with a speed of 20 mega samples per second.

Since a low-frequency perturbation causes very small modification of the Rayleigh scattering traces, a simple calculation of the differences between two neighboring successive traces is not enough to localize the perturbed fiber segment. **Figure 10** shows superposition of the absolute values of differences between all neighboring successive traces. One can see that the signal obtained for the distance of perturbations is the same as for any other positions.

However, the signal-to-noise ratio can be significantly improved with applying a special averaging procedure. For these purposes, we have processed the storage traces by employing three-step algorithm which is similar to moving differential method [19].

First, we determine the partial sums by averaging of N consequent traces. Each next partial sum is shifted by a number m of traces from the previous one. Then, we calculate the absolute value of the differences between every consequent partial sum.

The last step of the algorithm includes an analysis of the superposition of the absolute values for all differences.

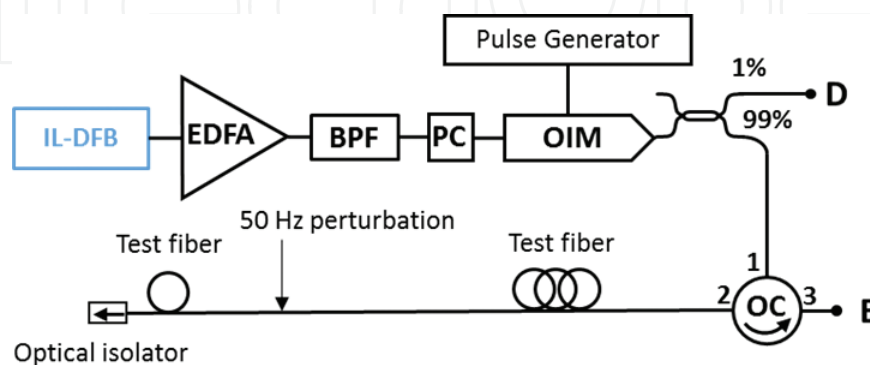


Figure 9. Experimental scheme for detection of the perturbation in the sensing fiber. BPF—Bandpass filter, PC—Polarization controller, OIM—Optical intensity modulator, OC—Optical circulator.

Figure 11 shows the superposition of all differences for $N = 75$ and $m = 10$. The highest peak denotes the point of the perturbation at 9270 m along the fiber under test. The signal peak exceeds the maximum of the noise value in 1.6 times and the average value of the noise approximately by 9 dB. Let us stress out that with the unlocked DFB laser, we never register the perturbation even at distances less than 0.1 km.

It is experimentally demonstrated that the relation between the signal and average value of the noise strongly depends on the shift between the averaging data arrays. However, a choice of

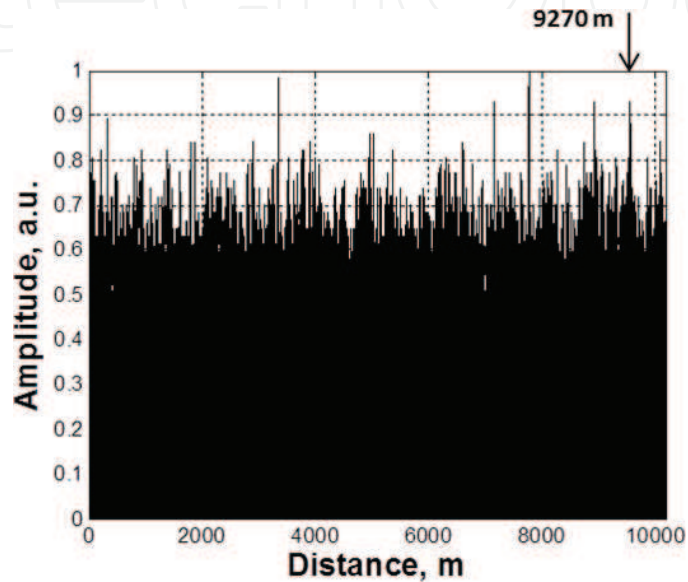


Figure 10. Superposition of the absolute values of differences between neighboring successive traces recorded with IL-DFB laser.

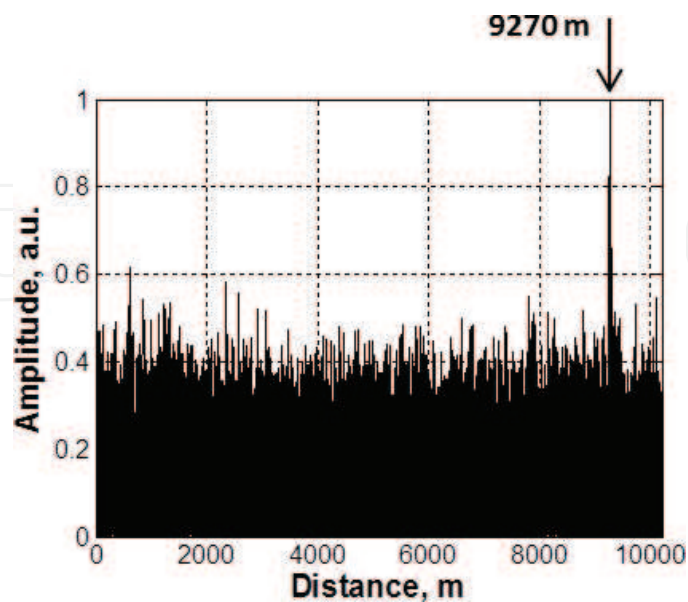


Figure 11. Superposition of the absolute values of differences between averaged traces for IL-DFB laser, $m = 10$ and $N = 75$.

the number of averaging not so strongly affects the signal-to-noise ratio and could be selected arbitrary within the interval between 40 and 120. **Figure 12** shows superposition of the absolute values of differences between the averaged traces for the shift $m = 23$ and averaging number $N = 75$.

The signal peak exceeds the maximum of the noise value in 2.1 times and the average noise value approximately by 10 dB.

Figure 13 shows a superposition of the absolute values of differences between the averaged traces for the shift of $m = 45$ and averaging number $N = 75$. The signal peak exceeds the maximum of the noise value in 1.4 times and the average noise value by approximately 8 dB.

A number of the performed experiments allow us to conclude that in our experimental conditions, the maximum of the signal-to-noise ratio is achieved with the shift m approximately equal to 20.

The obtained value of the signal-to-noise ratio allows correct localization of the perturbations with the IL-DFB laser system at distances of about 10 km and resolution of around 10–15 m but does not allow comparing a capacity of the proposed solution with commercially available techniques.

In order to fulfill this gap, we have performed the same measurements, under the same experimental conditions, but utilizing a commercially available ultra-narrow linewidth (~ 300 Hz) laser OEwaves laser OE4020–155000-PA-00. **Figure 14** shows the superposition of the subtractions of averaged traces for the measurements utilizing OEwaves laser for the shift $m = 23$ and averaging number $N = 75$. The signal peak at the distance of ~ 9270 m exceeds the highest noise signal in about 2.25 times that is nearly the same result as obtained with our IL-DFB laser.

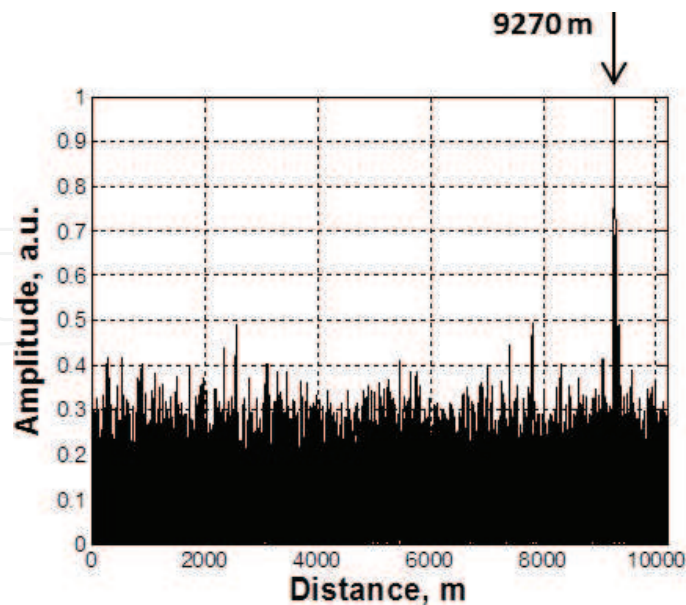


Figure 12. Superposition of the absolute values of differences between averaged traces for IL-DFB laser, $m = 23$ and $N = 75$.

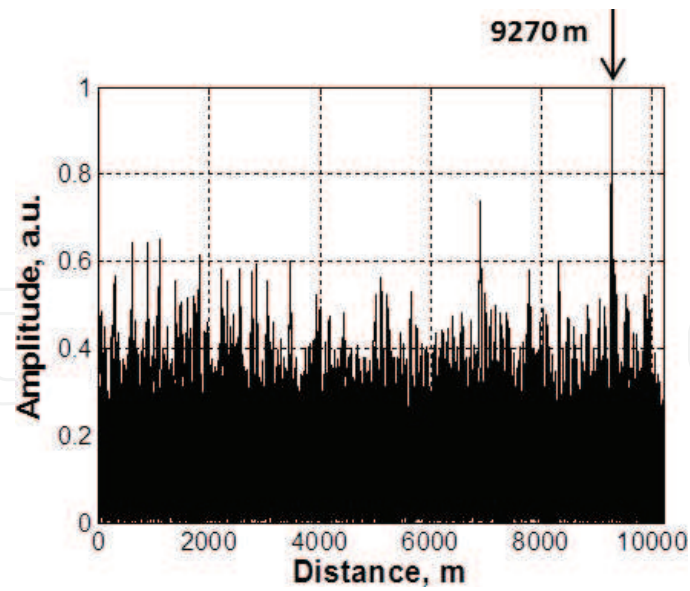


Figure 13. Superposition of the absolute values of differences between the averaged traces for IL-DFB laser, $m = 45$ and $N = 75$.

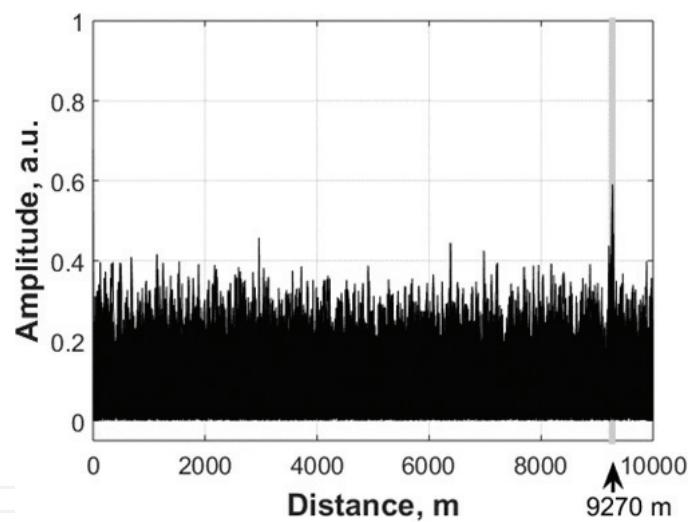


Figure 14. Superposition of the absolute values of the differences between average traces for ultra-narrow linewidth OEwaves laser OE4020-155000-PA-00.

3. Conclusion

We have employed IL-DFB laser configuration at the critical coupling regime for detection and localization of the perturbations by φ -OTDR system.

At the critical coupling regime, the laser power is practically totally accumulated inside the cavity providing strong feedback for laser locking and resulting in the best laser stability and

significant narrowing of the laser generation spectrum. The locked DFB laser with the linewidth of about 2.4 kHz provides the long-distance measurements of the perturbations as the moving differential processing algorithm is applied. The IL-DFB laser delivers accurate localization of vibrations at the frequency as low as low 50 Hz at the distance of ~9270 m with the same signal-to-noise ratio that is achieved with an expensive ultra-narrow linewidth laser OEwaves laser OE4020–155000-PA-00.

We believe that proposed solution can be useful for applications in cost-effective ϕ -OTDR system for the measurement of the perturbations at distances up to ten kilometers.

Acknowledgements

This work was supported by project N 265517 CONACYT, Mexico, Ministry of Education and Science of Russian Federation (14.Z50.31.0015, “State Assignment” 3.3889.2017), Russian Fund of Basic Research (16-42-732135 R-OFIM), and the IAP program VII/35 of the Belgian Science Policy. C.A. López-Mercado was sponsored by the CONACYT, Mexico as Postdoctoral Fellow at the University of Mons, Belgium.

Author details

Vasily V. Spirin^{1*}, Cesar A. López-Mercado², Patrice Mégret² and Andrei A. Fotiadi^{2,3,4}

*Address all correspondence to: vaspir@cicese.mx

1 División de Física Aplicada, CICESE, Ensenada, B.C., México

2 Electromagnetism and Telecommunication Department, University of Mons, Mons, Belgium

3 Ioffe Physico-Technical Institute of the RAS, St. Petersburg, Russia

4 Ulyanovsk State University, Ulyanovsk, Russia

References

- [1] Shi Y, Feng H, Zeng Z. Distributed fiber sensing system with wide frequency response and accurate location. *Optics and Lasers in Engineering*. 2016;**77**:219-224
- [2] Peng F, Wu H, Jia X-H, Rao YJ, Wang Z-N, Peng Z-P. Ultra-long high-sensitivity Φ -OTDR for high spatial resolution intrusion detection of pipelines. *Optics Express*. 2014;**22**:13804-13810
- [3] Spirin VV, Swart PL, Chtcherbakov AA, Miridonov SV, Shlyagin MG. Distributed fibre-optic loss sensor with chirped Bragg grating based on transmission-reflection analysis. *Electronics Letters*. 2003;**39**:895-897

- [4] López RM, Spirin VV, Shlyagin MG, Miridonov SV, Beltrán G, Kuzin EA, Márquez Lucero A. Coherent optical frequency domain reflectometry for interrogation of bend-based fiber optic hydrocarbon sensors. *Optical Fiber Technology*. 2004;**28**:79-90
- [5] Spirin VV, Mendieta FJ, Miridonov SV, Shlyagin MG, Chtcherbakov AA, Swart PL. Localization of a loss-inducing perturbation with variable accuracy along a test fiber using transmission-reflection analysis. *IEEE Photonics Technology Letters*. 2004;**16**:569-571
- [6] Spirin VV, Swart PL, Chtcherbakov AA, Miridonov SV, Shlyagin MG. 20-km length distributed fiber-optical loss sensor based on transmission - reflection analysis. *Optical Engineering*. 2005;**44**:040501
- [7] Spirin VV. Autonomous Measurement System for Localization of Loss-Induced Perturbation Based on Transmission-Reflection Analysis. In: Kr Sharma M, editor. *Advances in Measurement Systems*. InTech; 2010 ISBN 978-953-307-061-2, 81-104
- [8] Spirin VV, Shlyagin MG, Miridonov SV, Swart PL. Transmission/reflection analysis for distributed optical fibre loss sensor interrogation. *Electronics Letters*. 2002;**38**:117-118
- [9] Spirin VV, Shlyagin MG, Miridonov SV, Swart PL. Alarm-condition detection and localization using Rayleigh scattering for a fiber optic bending sensor with an unmodulated light source. *Optics Communications*. 2002;**205**:37-41
- [10] López RM, Spirin VV, Miridonov SV, Shlyagin MG, Beltrán G, Kuzin EA. Fiber optic distributed sensor for hydrocarbon leak localization based on transmission/reflection measurement. *Optics & Laser Technology*. 2002;**34**:465-469
- [11] Spirin VV. Transmission/reflection analysis for localization of temporally successive multi-point perturbations in distributed fiber-optic loss sensor based on Rayleigh backscattering. *Applied Optics-OT*. 2003;**42**:1175-1181
- [12] Bueno Escobedo JL, Spirin VV, López-Mercado CA, Lucero AM, Mégret P, Zolotovskii IO, Fotiadi AA. Self-injection locking of the DFB laser through an external ring fiber cavity: Application for phase sensitive OTDR acoustic sensor. *Results in Physics*. 2017;**7**:641-643
- [13] Wang C, Wang C, Shang Y, Liu X, Peng G. Distributed acoustic mapping based on interferometry of phase optical time-domain reflectometry. *Optics Communication*. 2015;**346**:172-177
- [14] Faustov A, Gussarov A, Wuilpart M, Fotiadi AA, Liokumovich LB, Kotov OI, Zolotovskiy IO, Tomashuk AL, Deschoutheete T, Mégret P. Distributed optical fibre temperature measurements in a low dose rate radiation environment based on Rayleigh backscattering. In: Berghmans F, Mignani AG, De Moor P, editors. *Proceedings of the SPIE 8439 Optical Sensing and Detection II*. 2012 pp. 84390C-84390C-8
- [15] Faustov AV, Gusarov AV, Mégret P, Wuilpart M, Zhukov AV, Novikov SG, Svetukhin VV, Fotiadi AA. The use of optical frequency-domain Reflectometry in remote distributed measurements of the γ -radiation dose. *Technical Physics Letters*. 2015;**41**(5):412-415
- [16] Faustov AV, Gusarov AV, Mégret P, Wuilpart M, Zhukov AV, Novikov SG, Svetukhin VV, Fotiadi AA. Application of phosphate doped fibers for OFDR dosimetry. *Results in Physics*. 2016;**6**:86-87

- [17] Faustov AV, Gusarov A, Wuilpart M, Fotiadi AA, Liokumovich LB, Zolotovskiy IO, Tomashuk AL, de Schoutheete T, Mégret P. Comparison of gamma-radiation induced attenuation in Al-doped, P-doped and Ge-doped fibres for Dosimetry. *IEEE Transactions on Nuclear Science*. 2013;**60**(4):2511-2517
- [18] Faustov AV, Andrei G, Liokumovich LB, Fotiadi AA, Wuilpart M, Mégret P. Comparison of simulated and experimental results for distributed radiation-induced absorption measurement using OFDR reflectometry. *Proc. SPIE*. 2013;**8794**:87943O
- [19] Lu Y, Zhu T, Chen L, Bao X. Distributed vibration sensor based on coherent detection of phase-OTDR. *Lightwave*. 2010;**28**:3243-3249
- [20] Li Q, Zhang C, Li L, Zhong X. Localization mechanisms and location methods of the disturbance sensor based on phase-sensitive OTDR. *Optik (Stuttg)*. 2014;**125**:2099-2103
- [21] Li Q, Zhang C, Li C. Fiber-optic distributed sensor based on phase-sensitive OTDR and wavelet packet transform for multiple disturbances location. *Optik (Stuttg)*. 2014;**125**:7235-7238
- [22] Zhan Y, Yu Q, Wang K, Yang F, Zhang B. Optimization of a distributed optical fiber sensor system based on phase sensitive OTDR for disturbance detection. *Sensor Review*. 2015;**35**:382-388
- [23] Spirin VV, Kellerman J, Swart PL, Fotiadi AA. Intensity noise in SBS with injection locking generation of stokes seed signal. *Optics Express*. 2006;**14**:8328-8335
- [24] Spirin VV, Kellerman J, Swart PL, Fotiadi AA. Intensity noise in SBS with seed signal generated through injection locking. *Conference Digest: CLEO-Europe'2007, IEEE*
- [25] Spirin VV, Castro M, López-Mercado CA, Mégret P, Fotiadi AA. Optical locking of two semiconductor lasers through high order Brillouin stokes components in optical Fiber. *Laser Physics*. 2012;**22**(4):760-764
- [26] Fotiadi AA, Kinet D, Mégret P, Spirin VV, Lopez-Mercado CA, Zolotovskii I. Brillouin Fiber Laser Passively Stabilized at Pump Resonance Frequency. *Symposium: IEEE Photonics Benelux Chapter; 2012*. pp. 365-368
- [27] Spirin VV, López-Mercado CA, Kinet D, Mégret P, Zolotovskiy IO, Fotiadi AA. Single longitudinal-mode Brillouin fiber laser passively stabilized at pump resonance frequency with dynamic population inversion grating. *Laser Physics Letters*. 2013;**10**:015102
- [28] Lopez-Mercado CA, Spirin VV, Zlobina EA, Kablukov SI, Mégret P, Fotiadi AA. Doubly-resonant Brillouin fiber cavity: Algorithm for cavity length adjustment. *IEEE Photonics Benelux Chapter*. 2012:369-372
- [29] Spirin VV, López-Mercado CA, Kinet D, Mégret P, Zolotovskiy IO, Fotiadi AA. Passively stabilized Brillouin fiber lasers with doubly resonant cavities. *Proceedings of SPIE*. 2013;**8601**:860135

- [30] Spirin VV, López-Mercado CA, Kinet D, Zlobina EA, Kablukov SI, Mégret P, Zolotovskiy IO, Fotiadi AA. Double-frequency Brillouin fiber lasers. Proc. SPIE 8772. 2013 87720U
- [31] Fotiadi A, Spirin V, López-Mercado C, Kinet D, Preda E, Zolotovskii I, Zlobina E, Kablukov S, Mégret P. Recent progress in passively stabilized single-frequency Brillouin fiber lasers with doubly-resonant cavities. CLEO/Europe and EQEC. CLEO-Europe: Conference Digest; 2013
- [32] Spirin VV, López-Mercado CA, Bueno-Escobedo JL, Lucero AM, Zolotovskii IO, Mégret P, Fotiadi AA. Self-injection locking of the DFB laser through ring fiber optic resonator. Proc. SPIE 9344. 2015 93442B
- [33] Lopez-Mercado CA, Spirin VV, Nava-Vega A, Patrice M, Andrei F. Láser de Brillouin con cavidad corta de fibra estabilizado pasivamente en la resonancia de bombeo por fenómeno de auto-encadenamiento por inyección óptica. Revista Mexicana de Física. 2014;**60**:53-58
- [34] Spirin VV, Mégret P, Fotiadi AA. Passively Stabilized Doubly Resonant Brillouin Fiber Lasers. In: Paul M, Kolkata J, editors. Fiber Lasers. InTech; 2016
- [35] Bueno Escobedo JL, Spirin VV, López-mercado CA, Mégret P, Zolotovskii IO, Fotiadi AA. Self-injection locking of the DFB laser through an external ring fiber cavity : Polarization behavior. Results in Physics. 2016;**6**:59-60
- [36] Spirin VV, López-Mercado CA, Mégret P, Fotiadi AA. Single-mode Brillouin fiber laser passively stabilized at resonance frequency with self-injection locked pump laser. Laser Physics Letters. 2012;**9**:377-380
- [37] López-Mercado CA, Spirin VV, Bueno Escobedo JL, Lucero AM, Mégret P, Zolotovskii IO, Fotiadi AA. Locking of the DFB laser through fiber optic resonator on different coupling regimes. Optics Communications. 2016;**359**:195-199
- [38] Faramarz E. Seraji, steady-state performance analysis of fiber-optic ring resonator. Progress in Quantum Electronics. 2009;**33**:1-16
- [39] Derickson D. Fiber Optic Test and Measurement. Prentice Hall PTR, c: Upper Saddle River, N.J; 1998
- [40] Muanenda Y, Oton CJ, Faralli S, Di Pasquale F. A cost-effective distributed acoustic sensor using a commercial off-the-shelf DFB laser and direct detection phase-OTDR. IEEE Photonics Journal. 2016;**8**:1-10
- [41] <http://www.corning.com/opticalfiber/index.asp>

